A Disubstituted Succinamide Is a Potent Sodium Channel Blocker with Efficacy in a Rat Pain Model

ARTICLE *in* BIOCHEMISTRY · SEPTEMBER 2004

Impact Factor: 3.02 · DOI: 10.1021/bi0493259 · Source: PubMed

A Disubstituted Succinamide Is a Potent Sodium Channel Blocker with Efficacy in a Rat Pain Model

Birgit T. Priest,[‡,@] Maria L. Garcia,[‡,@] Richard E. Middleton,[‡,@] Richard M. Brochu,[‡] Samantha Clark,[§] Ge Dai,[‡] Ivy E. Dick,[‡] John P. Felix,[‡] Chou J. Liu,[‡] Brita S. Reiseter,[||] William A. Schmalhofer,[‡] Pengcheng P. Shao,[⊥] Yui S. Tang,[▽] Margaret Z. Chou,[‡] Martin G. Kohler,[‡] McHardy M. Smith,[‡] Vivien A. Warren,[‡] Brande S. Williams,[‡] Charles J. Cohen,[‡] William J. Martin,[||] Peter T. Meinke,[⊥] William H. Parsons,[⊥] Keith A. Wafford,[§] and Gregory J. Kaczorowski*[,‡]

Departments of Ion Channels, Pharmacology, Drug Metabolism, and Medicinal Chemistry, Merck Research Laboratories, Rahway, New Jersey 07065

Received April 6, 2004; Revised Manuscript Received May 24, 2004

ABSTRACT: Sodium channel blockers are used clinically to treat a number of neuropathic pain conditions, but more potent and selective agents should improve on the therapeutic index of currently used drugs. In a high-throughput functional assay, a novel sodium channel (Na_V) blocker, *N*-{[2′-(aminosulfonyl)biphenyl-4-yl]methyl}-*N*′-(2,2′-bithien-5-ylmethyl)succinamide (BPBTS), was discovered. BPBTS is 2 orders of magnitude more potent than anticonvulsant and antiarrhythmic sodium channel blockers currently used to treat neuropathic pain. Resembling block by these agents, block of $Na_V1.2$, $Na_V1.5$, and $Na_V1.7$ by BPBTS was found to be voltage- and use-dependent. BPBTS appeared to bind preferentially to open and inactivated states and caused a dose-dependent hyperpolarizing shift in the steady-state availability curves for all sodium channel subtypes tested. The affinity of BPBTS for the resting and inactivated states of $Na_V1.2$ was 1.2 and 0.14 μM, respectively. BPBTS blocked $Na_V1.7$ and $Na_V1.2$ with similar potency, whereas block of $Na_V1.5$ was slightly more potent. The slow tetrodotoxin-resistant Na^+ current in small-diameter DRG neurons was also potently blocked by BPBTS. [^{3}H]BPBTS bound with high affinity to a single class of sites present in rat brain synaptosomal membranes (K_d = 6.1 nM), and in membranes derived from HEK cells stably expressing $Na_V1.5$ (K_d = 0.9 nM). BPBTS dose-dependently attenuated nociceptive behavior in the formalin test, a rat model of tonic pain. On the basis of these findings, BPBTS represents a structurally novel and potent sodium channel blocker that may be used as a template for the development of analgesic agents.

Voltage-gated ion channels enable electrically excitable cells to generate and propagate action potentials. Sodium channels play a unique role by mediating the rapid depolarization, which constitutes the rising phase of the action potential and in turn activates voltage-gated calcium and potassium channels. Nine sodium channel subtypes have been cloned and functionally expressed to date (*1*, *2*). In addition to the α-subunit (>200 kDa), sodium channels in many tissues contain one or two smaller β-subunits (*3*, *4*). In heterologous expression systems, the α-subunit alone forms functional sodium channels with all of the major properties of native channels: selectivity and voltage-dependent activation and inactivation. For some channel subtypes, coexpression with β-subunits results in higher expression levels, faster inactivation kinetics, or changes in steady-state voltage dependence (*5*−*8*).

Sodium channel α-subunits are the target of a range of pharmacological agents, including neurotoxins, antiarrhythmics, anticonvulsants, and local anesthetics (*9*). The S5 and S6 pore lining segments of sodium channels are involved in interactions with these agents, and these segments are highly conserved among different channel subtypes (*10*, *11*). Consistent with this finding, most sodium channel blockers known to date appear to interact with similar potency with all channel subtypes tested. Nevertheless, it has been possible to develop sodium channel blockers that display functional selectivity and an acceptable therapeutic index for the treatment of epilepsy (e.g., lamotrigine, phenytoin, and carbamazepine) and certain cardiac arrhythmias (e.g., lidocaine, tocainide, and mexiletine). The therapeutic index of these compounds is primarily a consequence of their use-dependent and state-dependent properties arising from higher binding affinity for open and inactivated states than for channels in resting closed states (*12*, *13*). More recently, sodium channel blockers have been used to treat a number of neuropathic pain conditions (*14*, *15*). Indeed, carbamazepine and a topical formulation of the local anesthetic lidocaine, Lidoderm, have been approved by the FDA for the treatment of trigeminal neuralgia and postherpetic neuralgia, respectively (*16*, *17*).

* To whom correspondence should be addressed: Phone: (732) 594-7565. Fax: (732) 594-3925. E-mail: gregory_kaczorowski@merck.com.
[‡] Department of Ion Channels.
[§] Neuroscience Research Centre, Merck Sharp and Dohme Research Laboratories, Terlings Park, Eastwick Rd., Harlow, Essex CM20 2QR, U.K.
[||] Department of Pharmacology.
[⊥] Department of Medicinal Chemistry.
[▽] Department of Drug Metabolism.
[@] These authors contributed equally to this work.

10.1021/bi0493259 CCC: $27.50
Published on Web 00/00/0000 PAGE EST: 10.6

Despite the obvious therapeutic potential of sodium channel blockers, few novel chemical entities have been discovered since the cloning of the first sodium channel in 1984 (*18*). The lack of new sodium channel blockers is largely due to a lack of appropriate high-throughput assays. To date, the only commercially available high-affinity radioligands are tetrodotoxin (TTX),[1] saxitoxin (STX), and batrachotoxinin A 20-α-benzoate (BTX-B). TTX and STX have very low affinity for $Na_V1.8$ and $Na_V1.9$, two sodium channel subtypes predominantly expressed in nociceptive neurons and of interest as potential pain targets (*19*−*22*). More importantly, TTX and STX are external pore blockers that interact with the channel independent of its gating conformation, and may not compete with state-dependent blockers of therapeutic usefulness (*23*). [^{3}H]BTX-B can be used to monitor binding of known classes of state-dependent blockers, since the BTX-B binding site is allosterically coupled to other drug binding sites on the channel. However, coapplication of scorpion toxin is required to enhance specific binding of [^{3}H]BTX-B, which may complicate assay results (*24*). Known anticonvulsants and local anesthetics are state-dependent blockers and appear to bind to a common site or overlapping sites within the pore (*11*); however, they are not high-affinity ligands and, therefore, are not suitable for binding assays. Electrophysiology has been the standard functional assay for sodium channels, but the extremely low throughput of this assay has limited its use to the detailed characterization of a few chosen compounds. Recent advances in fluorescence-based membrane-potential assays (*25*) and automated voltage clamp technologies (*26*) have enabled high- and medium-throughput functional evaluation of sodium channel blockers, respectively.

In this paper we report a structurally novel, state-dependent sodium channel blocker, BPBTS, that is active in a high-throughput fluorescence-based assay, with potency ∼50-fold greater than that of lidocaine, and that displays efficacy in a rat tonic pain model. [^{3}H]BPBTS binds with high affinity to a receptor site associated with sodium channels in brain and in HEK cells transfected with $hNa_V1.5$. Given its properties, BPBTS represents a potential lead for the development of new agents that selectively target sodium channels.

MATERIALS AND METHODS

Materials. An HEK-293 cell line stably expressing $hNa_V1.2$ together with the sodium channel β1 subunit was established in-house. Stable HEK-293 cell lines expressing $hNa_V1.5$ or $hNa_V1.7$ were obtained from Dr. Hartman and Aurora Biosciences, respectively. All tissue culture media were from Invitrogen Corp., Carlsbad, CA. For electrophysiological recordings, cells were plated on 35 mm dishes coated with poly-D-lysine. CC2-DMPE and $DiSBAC_2$ were purchased from Invitrogen. Tetracaine hydrochloride, quinidine, flunarizine, phenytoin, lidocaine, and TTX were from Sigma-Aldrich, Saint Louis, MO. Veratridine and (*R*)-SDZ-201 were from Biomol Research Laboratory Inc., Plymouth Meeting, PA. Brevetoxin was from CalBiochem, San Diego, CA, and deltamethrin from Crescent Chemical Corp., Islandia, NY. WIN 17317-3 was prepared as previously described (*27*).

VIPR Assay. The VIPR (voltage/ion probe reader; *28*) assay was performed as described previously (*29*). Briefly, $hNa_V1.2$, $hNa_V1.5$, or $hNa_V1.7$ cells were plated at approximately 100000 cells/well in poly-D-lysine-coated 96-well plates and incubated overnight at 37 °C. Cells were stained with voltage-sensitive dyes by being incubated in Dulbecco's phosphate-buffered saline (DPBS) supplemented with 10 mM glucose, 10 mM HEPES−Na (pH 7.5), and 10 μM CC2-DMPE for 0.7 h at 27 °C, rinsed with Na-free medium (160 mM tetramethylammonium chloride, 0.1 mM $CaCl_2$, 1 mM $MgCl_2$, 11 mM glucose, 10 mM HEPES−K, pH 7.5, [K^+] approximately 4.5 mM), and then incubated in Na-free medium supplemented with 10 μM $DiSBAC_2$, sodium channel agonist(s), and the test sample, at the indicated concentration for 0.7 h at 27 °C. The sodium channel agonists used were 20 μM veratridine for $Na_V1.5$, 20 μM veratridine and 20 nM $PbTx_3$ for $Na_V1.7$, and 20 μM veratridine and 20 μM deltamethrin for $Na_V1.2$. Cells were placed in the VIPR plate reader and illuminated at 400 nm, and fluorescence emissions at 460 and 580 nm were recorded at 1 Hz. After a 7 s baseline, Na solution was added (165 mM NaCl, 4.5 mM KCl, 2 mM $CaCl_2$, 1 mM $MgCl_2$, 11 mM glucose, 10 mM HEPES−Na, pH 7.5) to give a final Na concentration of approximately 85 mM, and the change in fluorescence resonance energy transfer (FRET) ratio was recorded. Background fluorescence was not subtracted.

DRG Preparation. DRGs were dissected from BKTO mice following cervical dislocation in accordance with the UK Animals (Scientific Procedures) Act (1986) and its associated guidelines. Ganglia from all levels were placed into Hanks solution containing 45 units/mL papain and 0.4 mg/mL L-cysteine for 15 min at 37 °C, followed by 2 mg/mL collagenase (type I) in Hanks solution for 15−18 min at 37 °C. The ganglia were washed once with growth medium (F14, 10% horse serum, Pen/strep (5000 IU/500 μg), 120 mg of $NaHCO_3$, and 100 ng/mL NGF) and triturated with a fire-polished pipet to obtain a single cell suspension which was plated onto poly-L-ornithine-coated glass coverslips. All recordings were made within 2−8 h of ganglia isolation.

Electrophysiology. Sodium currents were examined by whole cell voltage clamp (*30*) using either an EPC-9 amplifier and Pulse software (HEKA Electronics, Lamprecht, Germany) or an Axopatch 200B amplifier and pClamp7 software (Axon Instruments, Foster City, CA). Experiments were performed at room temperature. Electrodes were fire-polished to resistances of 1.5−4 MΩ. Voltage errors were minimized by series resistance compensation (75−85%), and the capacitance artifact was canceled using the amplifier's built-in circuitry. Data were acquired at 10−50 kHz and filtered at 5−10 kHz. For recombinant channels expressed in HEK cells, the bath solution typically consisted of 40 mM NaCl, 120 mM NMDG−Cl, 1 mM KCl, 2.7 mM $CaCl_2$, 0.5 mM $MgCl_2$, and 10 mM NMDG−HEPES, pH 7.4, and the internal (pipet) solution contained 110 mM cesium methanesulfonate, 5 mM NaCl, 20 mM CsCl, 10 mM CsF, 10

[1] Abbreviations: AUC, area under the curve; BAPTA, 1,2-bis(2-aminophenoxy)ethane-*N*,*N*,*N*′,*N*′-tetraacetic acid; BKTO, Bantin and Kingman Tyler's outbred; BPBTS, *N*-{[2′-(aminosulfonyl)biphenyl-4-yl]methyl}-*N*′-(2,2′-bithien-5-ylmethyl)succinamide; BTX-B, batrachotoxin A 20-α-benzoate; DRG, dorsal root ganglion; EtOAc, ethyl acetate; FRET, fluorescence resonance energy transfer; HEPES, *N*-(2-hydroxyethyl)piperazine-*N*′-(2-ethanesulfonic acid); Na_V, voltage-dependent sodium channel; NGF, nerve growth factor; NMDG, *N*-methyl-D-glucamine; $PbTx_3$, brevetoxin; STX, saxitoxin; TEA, tetraethylammonium; THF, tetrahydrofuran; TTX, tetrodotoxin; VIPR, voltage/ion probe reader; WIN 17317-3, 1-benzyl-7-chloro-4-(*n*-pentylimino)-1,4-dihydroquinoline hydrochloride.

Scheme 1[a]

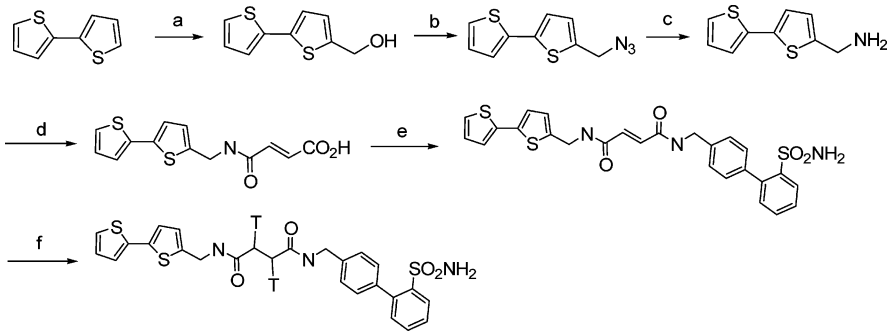

[a] Reagents and conditions: (a) (1) *n*-buytllithium, THF, −78 °C, (2) $(CHO)_n$, −78 °C to room temperature; (b) DPPA, DEAD, THF; (c) PPh_3, THF, H_2O; (d) maleic anhydride, dioxane; (e) [2′-(aminosulfonyl)biphenyl-4-yl]methylamine, BOP, DIEA, THF; (f) tritium gas, 380−120 mmHg, 10% Pd/C, DMF, room temperature, 2 h.

mM BAPTA (tetracesium salt), and 10 mM Cs−HEPES, pH 7.4. In some cases, NMDG−Cl in the bath solution was replaced by NaCl to increase current amplitudes. To isolate TTX-resistant Na^+ current in DRG neurons, the bath solution contained 40 mM NaCl, 50 mM TEA−Cl, 40 mM choline chloride, 0.1 mM $CaCl_2$, 3.9 mM $MgCl_2$, 10 mM TEA−HEPES, 11 mM glucose, and 300 nM TTX, pH 7.4, and the internal solution contained 115 mM CsF, 10 mM NaCl, 3.9 mM $MgCl_2$, 10 mM BAPTA (tetracesium salt), and 10 mM Cs−HEPES, pH 7.3, adjusted to 300 mOsm with sucrose. Liquid junction potentials were less than 4 mV and were not corrected for. Unless otherwise stated, the holding potential was −90 mV. Steady-state availability curves were generated using 10 s conditioning prepulses to allow sufficient time for drug to equilibrate at each prepulse potential. The maximum current available upon depolarization from negative holding potentials (I_{max}) and the difference in the midpoints of the steady-state availability curves (ΔV) in the control and in the presence of a compound were used to calculate the steady-state affinity of compounds for the resting and inactivated states of the channel (K_r and K_i, respectively) using the following equations as previously described for lidocaine block of cardiac channels (*31*):

$$K_r = \frac{[\text{drug}]I_{\text{max,drug}}}{I_{\text{max,control}} - I_{\text{max,drug}}}$$

$$K_i = \frac{[\text{drug}]}{\left(1 + \frac{[\text{drug}]}{K_r}\right)e^{-\Delta V/k} - 1}$$

All averaged data are presented as mean ± standard error. Statistical comparisons were made using Student's *t* test, and differences were considered significant at $P < 0.05$.

Synthesis of [^{3}H]BPBTS (Scheme 1). (a) Preparation of 2,2′-Bithien-5-ylmethylamine. (1) 2,2′-Bithien-5-ylmethanol. To a stirred solution of 21 g (0.13 mol) of 2,2′-bithiophene (Aldrich Chemical Co., Milwaukee, WI) in 250 mL of THF at −78 °C was added over a period of 30 min 79 mL of *n*-butyllithium (1.6 M solution in hexanes, 0.13 mol). After the solution was stirred for 3 h at −78 °C, 4.55 g (0.15 mol) of paraformaldehyde was added, and the resulting reaction mixture was allowed to slowly warm to room temperature. After being stirred at room temperature for 18 h, the reaction mixture was partitioned between H_2O and ethyl acetate. The aqueous layer was extracted twice with EtOAc, and the combined organic fractions were concentrated. The residue was purified by chromatography (silica, 3:7 EtOAc/hexanes) to give 2,2′-bithien-5-ylmethanol.

(2) 2,2′-Bithien-5-ylmethyl Azide. A solution of 0.5 g (2.55 mmol) of 2,2′-bithien-5-ylmethanol, 0.824 mL (0.31 mol) of diphenylphosphoryl azide (DPPA), 0.48 mL (3.1 mmol) of diethylazodicarboxylate (DEAD), and 0.8 g (3.1 mmol) of triphenylphosphine (PPh_3) in 10 mL of THF was stirred at room temperature for 18 h. The resulting reaction mixture was diluted with dichloromethane, washed three times with H_2O and once with brine solution, dried ($MgSO_4$), and filtered, and the filtrate was concentrated. The residue was purified by chromatography (silica, 5:95 EtOAc/hexanes) to give 2,2′-bithien-5-ylmethyl azide.

(3) 2,2′-Bithien-5-ylmethylamine. A mixture of 2.78 g (12.6 mmol) of 2,2′-bithien-5-ylmethyl azide and 4.95 g (19 mmol) of triphenylphosphine in 20 mL of THF and 2 mL of H_2O was stirred at room temperature for 18 h. The resulting reaction mixture was concentrated, and the residue was purified by chromatography (silica, 5:95:0.1 EtOAc/hexanes/NH_4OH) to give 2.1 g of 2,2′-bithien-5-ylmethylamine: ^{1}H NMR (500 MHz, CD_3OD) δ 7.28 (dd, 1H, J = 1 and 5 Hz), 7.15 (dd, 1H, J = 1 and 4 Hz), 7.03 (m, 2H), 6.88 (d, 1H, 4 Hz).

(b) Preparation of [2′-(Aminosulfonyl)biphenyl-4-yl]methylamine. [4-(2-Aminosulfonylphenyl)]benzylamine was synthesized as previously reported (*32*).

(c) Preparation of [^{3}H]-N-{[2′-(Aminosulfonyl)biphenyl-4-yl]methyl}-N′-(2,2′-bithien-5-ylmethyl)succinamide. A solution of 0.05 g (0.51 mmol) of maleic anhydride and 0.1 g (0.51 mmol) of 2,2′-bithien-5-ylmethylamine in 3 mL of dioxane was stirred at room temperature for 2 h. The reaction mixture was then concentrated, and the residue was purified by chromatography (HPLC, Waters YMC-Pack Pro C18 column, H_2O/CH_3CN gradient) to give 0.11 g of 4-[2,2′-bithien-5-ylmethylamino]-4-oxobut-2-enylcarboxylic acid. A mixture of 0.02 g (0.068 mmol) of 4-[2,2′-bithien-5-ylmethylamino]-4-oxobut-2-enylcarboxylic acid, 0.018 g (0.068 mmol) of [2′-(aminosulfonyl)biphenyl-4-yl]methylamine, 0.036 g (0.082 mmol) of benzotriazol-1-yloxytris-(dimethylamino)phosphonium hexafluorophosphate, and 47 μL of diisopropylethylamine (DIEA) in 2 mL of THF was stirred at room temperature for 3 h. The reaction mixture was concentrated, and the residue was purified by chromatography (HPLC, Waters YMC-Pack Pro C18 column, H_2O/CH_3CN gradient) to give 0.025 g of the maleic acid

diamide: MS (ESI) *m/e* 560 (M + 1). A solution of 6 mg of this diamide in 0.8 mL of *N*,*N*-dimethylformamide (DMF) was degassed at dry ice/acetone temperature in the presence of 5 mg of 10% Pd/C and then stirred at room temperature for 2 h under 380−120 mmHg of carrier-free tritium gas. The catalyst and any unreacted tritium gas were removed, and the solvent and labile tritiums were concentrated to near dryness. The dried residue was resuspended in 2 mL of ethanol, and the title compound was purified by HPLC (Phenomenex phenylhexyl column, CH_3CN/H_2O/TFA, 20:80:0.1 to 25:75:0.1 in 25 min). The title compound was eluted with a retention time of 16 min, was 99% radiochemically pure, and had a specific activity of 32.9 Ci/mmol.

Binding Assay. Rat brain synaptosomal plasma membrane vesicles and membranes from HEK-293 cells stably transfected with $hNa_V1.5$ were prepared as previously described (*33*), and stored at −70 °C. Binding of [^{3}H]BPBTS was monitored at room temperature in 20 mM Tris−HCl, pH 7.4, with 0.01 mg/mL bacitracin. For saturation experiments, membranes were incubated with [^{3}H]BPBTS at room temperature for at least 5 h. To determine the kinetics of ligand association, membranes were incubated with [^{3}H]BPBTS for different periods of time at room temperature. Dissociation kinetics were initiated by addition of 1−10 μM unlabeled BPBTS. Nonspecific binding was determined in the presence of 1 μM unlabeled BPBTS. Separation of bound from free ligand was achieved by diluting samples with 4 mL of ice-cold buffer consisting of 10 mM Tris−HCl, pH 7.4, and 0.1% Triton-X100 and filtering through GF/C glass fiber filters presoaked in 0.5% polyethylenimine. Radioactivity retained on the filters was determined by liquid scintillation techniques. Data from saturation experiments were analyzed according to the equation $B_{eq} = (B_{max}L^*)/(K_d + L^*)$, where B_{eq} is the amount of ligand bound at equilibrium, B_{max} the maximum receptor concentration, K_d the ligand dissociation constant, and L^* the free ligand concentration. The association rate constant (k_1) was determined from the equation $k_1 = k_{obs}(B_{eq}/(L^*B_{max}))$, where k_{obs} is the slope of the pseudo-first-order plot $\ln(B_{eq}/(B_{eq} - B_t))$ versus time. The dissociation rate constant k_{-1} was calculated by fitting the data to a single monoexponential decay. IC_{50} values for inhibition of [^{3}H]-BPBTS binding were determined using the equation $B_{eq} = (B_{max} - B_{min})/[1 + (I/IC_{50})^{nH}] + B_{min}$, where B_{max} is the amount of ligand bound with no inhibitors present, B_{min} is the amount of ligand bound at the maximal inhibitor concentration, I is the inhibitor concentration, nH is the Hill coefficient, and IC_{50} is the inhibitor concentration resulting in 50% inhibition. In most experiments, B_{max} was approximately 100% and B_{min} was typically close to 0%.

Formalin Test. All experimental protocols were in accordance with the NIH guidelines for the use of live animals and were approved by the Merck Research Laboratories−Rahway Institutional Animal Care and Use Committee. Separate groups of 4−20 male Sprague−Dawley rats (Charles River, 200−250 g) were used for each experiment. A metal band was affixed to the left hind paw, and each rat was conditioned to the band for 60 min within a plastic cylinder (15 cm diameter). BPBTS was prepared in a 1:4:5 vehicle of ethanol, PEG400, and saline (EPEGS) and injected subcutaneously into the dorsal surface of the left hind paw 5 min prior to injection of 50 μL of 5% formalin. Alternatively, BPBTS was given intravenously either 5 min prior to or 15 min after formalin injection. Flinches were counted continuously for 60 min using an automated nociception analyzer (UCSD Anesthesiology Research, San Diego, CA). Statistical significance was determined by comparing the total flinches detected in vehicle- and BPBTS-treated animals with an unpaired *t* test or a one-way ANOVA.

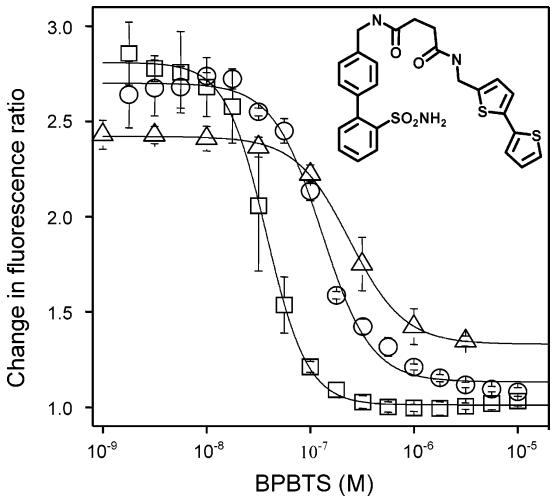

FIGURE 1: Inhibition of sodium-channel-dependent depolarization by BPBTS. Voltage-sensitive FRET between a pair of membrane-bound fluorescent dyes was used to monitor changes in membrane potential upon addition of Na to cells, preincubated with veratridine and varying concentrations of BPBTS. The FRET ratio is shown as a function of BPBTS concentration for stable cell lines expressing $hNa_V1.2$ (△), $hNa_V1.5$ (□), and $hNa_V1.7$ (○). Fitting to the Hill equation with a Hill coefficient of 1 yielded IC_{50} values of 380, 40, and 130 nM for $hNa_V1.2$, $hNa_V1.5$, and $hNa_V1.7$, respectively.

RESULTS

Identification of N-{[2′-(Aminosulfonyl)biphenyl-4-yl]-methyl}-N′-(2,2′-bithien-5-ylmethyl)succinamide, a Novel Voltage-Gated Sodium Channel Blocker. A high-throughput functional assay was used to screen the in-house sample collection for structurally novel sodium channel blockers. This assay uses voltage-dependent FRET between a pair of membrane-bound fluorescent probes to monitor changes in membrane potential. Cells are incubated with channel agonists and test compounds in the absence of sodium, then depolarization is initiated by sodium addition, and changes in FRET are monitored. The assay identified *N*-{[2′-(aminosulfonyl)biphenyl-4-yl]methyl}-*N*′-(2,2′-bithien-5-ylmethyl)succinamide as a novel sodium channel blocker, structurally unrelated to known channel blockers (Figure 1 inset). The compound herein referred to as BPBTS (biphenylbithienylsuccinamide) potently inhibits the Na_V1-mediated depolarization measured in FRET assays using HEK-293 cells stably expressing $Na_V1.2$, $Na_V1.5$, or $Na_V1.7$. Figure 1 shows the depolarization-induced increase in the 460/580 nm fluorescence emission ratio (decrease in FRET) as a function of BPBTS concentration. The solid lines represent the best fit of the data to the Hill equation with a Hill coefficient of 1. Average IC_{50} values were 341 ± 116 nM (n = 5), 46 ± 17 nM (n = 6), and 148 ± 43 nM (n = 8) for $Na_V1.2$, $Na_V1.5$, and $Na_V1.7$, respectively. The potencies of TTX against $hNa_V1.7$ and $hNa_V1.5$ measured in this assay, 33 ± 21 nM and 15 ± 10 μM, respectively (data not shown), were in agreement with the known TTX sensitivity of these channels (*34*−*36*). To determine its selectivity for Na_V1

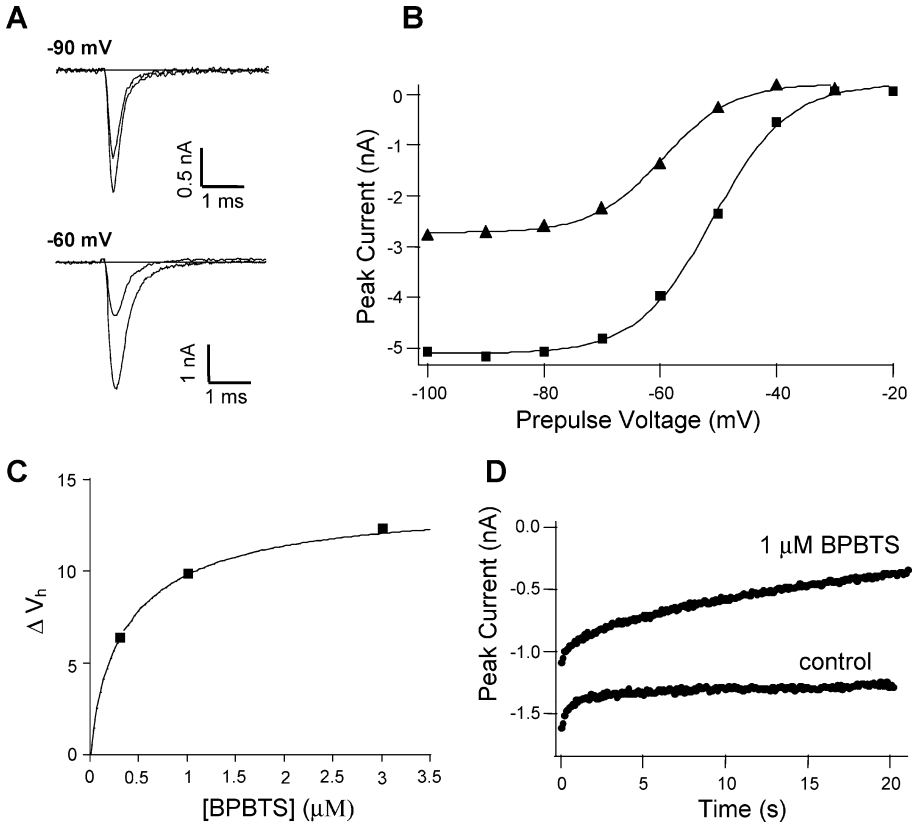

FIGURE 2: Block of hNa$_V$1.2 by BPBTS. Block of hNa$_V$1.2 channels stably expressed in HEK cells was examined by whole cell voltage clamp. (A) Current traces elicited by steps to 0 mV from −90 mV (top) or −60 mV (bottom) in the control and in the presence of 1 μM BPBTS. (B) Peak current elicited by pulses to 0 mV as a function of the prepulse potential in the control (squares) and in 1 μM BPBTS (triangles). Data were fitted to the Boltzmann equation, yielding in the control $I_{max} = -5.32$ nA, $V_h = -51.0$ mV, and $k = 6.5$ mV and in 1 μM BPBTS $I_{max} = -2.94$ nA, $V_h = -59.6$ mV, and $k = 6.0$ mV. (C) BPBTS-induced shift in the midpoint of the availability curves as a function of BPBTS concentration. Fitting the data to $V_h = (-5.8 \text{ mV}) \ln((1 + ([\text{BPBTS}]/K_r))/(1 + ([\text{BPBTS}]/K_i)))$ yielded $K_r = 1.3$ μM and $K_i = 0.11$ μM. (D) Use-dependent block of hNa$_V$1.2 during 10 Hz stimulation with 6 ms pulses to 0 mV from −100 mV.

channels, BPBTS was tested in radioligand binding assays against other ion channels as well as numerous receptors and enzymes. BPBTS, at 10 μM, did not affect [^{3}H]diltiazem binding to L-type calcium channels in rabbit skeletal muscle membranes. BPBTS (1 and 10 μM) inhibited [^{3}H]MK-0499 binding to membranes derived from HEK cells stably expressing HERG by 8% and 63%, respectively. Evaluation of BPBTS (10 μM) in over 100 receptor ligand binding and enzymatic assays in a standard PanLabs screen (MDS Pharma Services, Taiwan) yielded few significant interactions, the most potent being inhibition of ligand binding to thromboxane A_2 ($IC_{50} = 0.51$ μM), followed by several transporters with IC_{50} values in the 1−5 μM range, and the cannabinoid receptor CB1 ($IC_{50} = 4.5$ μM). Thus, within the limitations of these assays, BPBTS appears to be selective for sodium channels.

Block of Recombinant Na$_V$1.2 Channels by BPBTS. BPBTS was further characterized in whole cell electrophysiology, where bath application of 1 μM BPBTS reversibly blocked Na$_V$1.2 channels in a voltage-dependent manner as shown in Figure 2A. The current evoked by 6 ms depolarizations to 0 mV from −90 mV was blocked 34% by 1 μM BPBTS, whereas the current evoked by the same test pulse from a holding potential of −60 mV was blocked by 58%. The time course of block was similar at the two holding potentials and did not require depolarizing pulses, since block occurred with a similar time course during 0.5 and 0.017 Hz stimulation (data not shown). Since BPBTS does not carry a charge, the dependence of block on holding potential likely results from preferential interaction with channel states favored by membrane depolarization. This type of state-dependent block occurs with local anesthetics and has been described in detail. A hallmark of this mechanism is a drug-dependent shift in the voltage dependence of steady-state availability/inactivation to more hyperpolarized potentials, as is shown for Na$_V$1.2 channels in the absence and presence of 1 μM BPBTS (Figure 2B). The maximum current available on depolarization from negative holding potentials was reduced by 45% in the presence of 1 μM BPBTS, suggesting an IC_{50} of the compound for binding to the resting state of the channel (K_r) of 1.2 ± 0.1 μM ($n = 4$). In addition to the effect on the resting state, 1 μM BPBTS shifted the midpoint of the steady-state availability curve (V_h) by −8.6 mV. This shift was concentration-dependent (Figure 2C). Application of 1 and 0.3 μM BPBTS resulted in average shifts of −9.9 mV ($n = 2$) and −6.4 mV ($n = 2$), respectively, whereas 3 μM BPBTS caused a −12.4 mV shift in the steady-state availability curve. Assuming a simple two-state model where drug can bind with different affinities to either the resting (K_r) or inactivated (K_i) state of the channel, the concentration dependence of the shift in V_h is described by the equation $\Delta V_h = k \ln((1 + [\text{drug}]/K_r)/(1 + [\text{drug}]/K_i))$, where k is the slope of the Boltzmann equation describing the availability curve. Fixing k at −5.8 mV, the average slope of the control availability curves, and fitting the data in Figure 2C to this equation yielded $K_r = 1.3$ μM

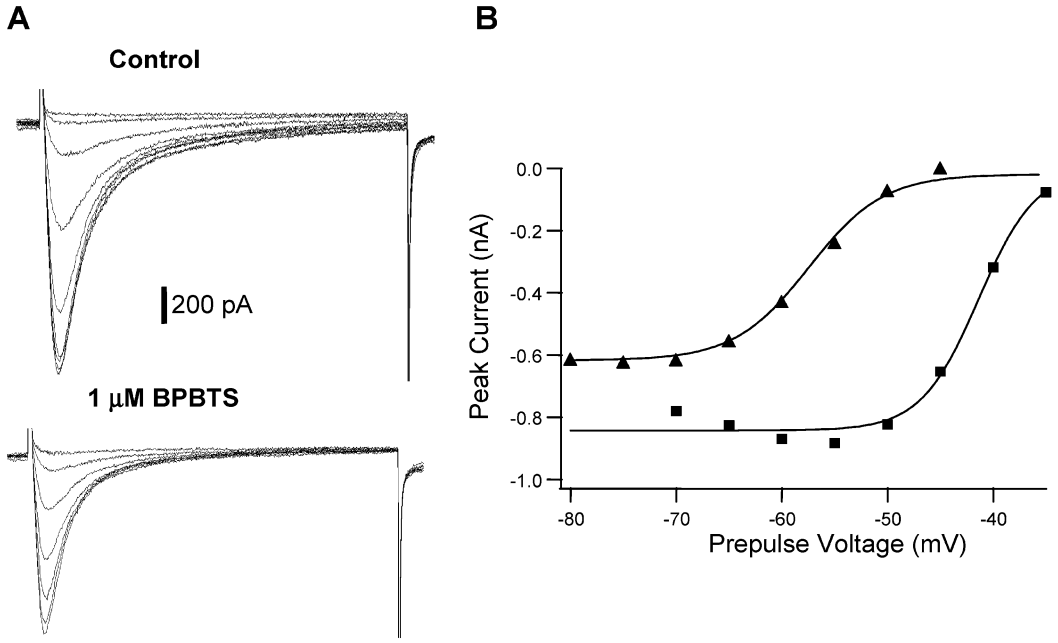

FIGURE 3: Block of TTX-resistant sodium current in mouse DRGs. Acutely dissociated small-diameter DRGs were examined by whole cell voltage clamp in the presence of 300 nM TTX. (A) Current traces elicited by 40 ms pulses to −10 mV from holding potentials of −80 to −30 mV in the control (top panel) and in 1 μM BPBTS (bottom panel). (B) Peak current elicited by pulses to −10 mV as a function of the prepulse potential in the control (squares) and in 1 μM BPBTS (triangles). Data were fitted to the Boltzmann equation, yielding in the control $I_{max} = -0.86$ nA, $V_h = -41.5$ mV, and $k = 2.8$ mV and in 1 μM BPBTS $I_{max} = -0.63$ nA, $V_h = -56.5$ mV, and $k = 4.0$ mV.

and $K_i = 0.11$ μM. The close agreement of these data with the average K_r of 1.2 μM supports the validity of the model. Data from a larger concentration range would have been desirable, but were precluded by the comparatively high affinity for the resting state, not leaving enough current at higher drug concentrations to reliably measure steady-state availability, and by the relatively slow kinetics of block at low drug concentrations. When K_i was calculated separately for each experiment (see the Materials and Methods), the average value was 0.14 ± 0.03 μM. As might be expected from the apparent state dependence of block, BPBTS displayed use-dependent block of $Na_V1.2$ as shown in Figure 2D. During 10 Hz stimulation, 1 μM BPBTS caused significant use-dependent block in addition to tonic block seen at the holding potential of −90 mV. Use-dependent or phasic block developed over more than 20 s and was fitted well by a double exponential. The fast phase with a time constant of 0.74 s accounted for 14% of the initial current and was also seen in the absence of BPBTS (0.77 s and 16%). The second phase was only seen in the presence of BPBTS and developed slowly with a time constant of 18 s. Stimulation was interrupted before block had reached steady state, but on the basis of the exponential fit, block was expected to reach 88%.

Block of Recombinant $Na_V1.5$ and $Na_V1.7$ Channels. Results from the VIPR assay suggested that BPBTS blocks $Na_V1.2$, $Na_V1.5$, and $Na_V1.7$ channels with similar potency. Whole cell voltage clamp experiments were carried out to examine the state dependence of block of $Na_V1.5$ and $Na_V1.7$ channels (Table 1). BPBTS blocked the resting states of $Na_V1.2$ and $Na_V1.7$ channels with similar potency, whereas block of the resting state of $Na_V1.5$ channels was approximately 4-fold more potent ($P < 0.05$). As shown for $Na_V1.2$, BPBTS appeared to bind with higher affinity to inactivated than to resting states of both $Na_V1.5$ and $Na_V1.7$ channels. The apparent affinity for the inactivated state was slightly higher for $Na_V1.5$ channels ($K_i = 0.08$ μM) than for $Na_V1.2$ and $Na_V1.7$ channels ($K_i = 0.14$ and 0.15 μM, respectively), although the difference was not statistically significant ($P > 0.1$).

Table 1: BPBTS Block of $Na_V1.2$, $Na_V1.5$ and $Na_V1.7$ Channels

	K_r (μM)			K_i (μM)			block with 10 Hz stimulation[a]
	mean	std error	*n*	mean	std error	*n*	(%)
$Na_V1.2$	1.2	0.1	4	0.14	0.03	5	88
$Na_V1.5$	0.3	0.1	4	0.08	0.01	4	94
$Na_V1.7$	1.3	0.4	10	0.15	0.06	9	85

[a] Determined from exponential fits to 20 s recordings in 1 μM BPBTS at −100 mV.

Block of the TTX-Resistant Current in Mouse DRGs. Several lines of experimental evidence have implicated TTX-resistant currents in the hyperexcitability of small-diameter sensory neurones resulting from inflammation or nerve injury (*37*, *38*). To examine block of this current by BPBTS, dorsal root ganglia were isolated from BKTO mice and acutely dissociated. Whole cell recordings were conducted on small-diameter neurons (10−25 μm diameter) using solutions designed to isolate sodium currents. TTX, at 300 nM, was used in all studies to isolate the TTX-resistant sodium current. Under these conditions, peak current amplitudes ranged from −0.5 to −2.5 nA, allowing for adequate voltage control of the cell. Figure 3A shows representative current traces activated by 40 ms pulses to −10 mV from holding potentials ranging from −80 to −30 mV. Currents show the relatively slow inactivation kinetics characteristic of native TTX-resistant currents. Availability curves generated from similar data had an average midpoint and slope of −43.1 and −2.8 mV, respectively. After bath equilibration with 1 μM BPBTS the maximum current activated by pulses to −10 mV from hyperpolarized holding potentials was significantly reduced

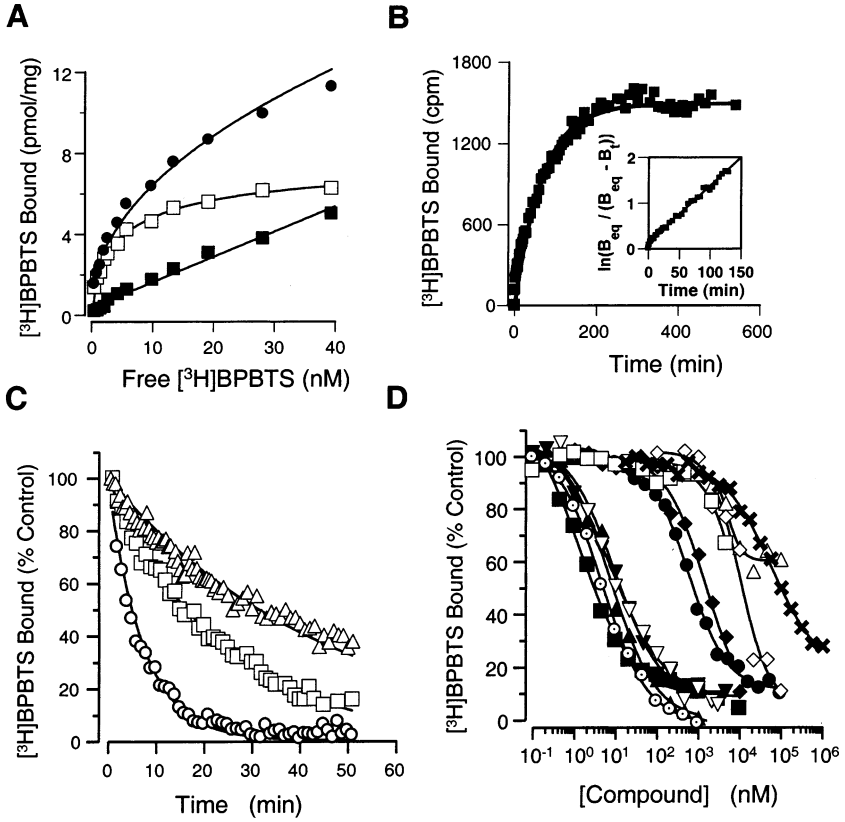

FIGURE 4: Binding of [^{3}H]BPBTS to rat brain synaptosomal membranes. (A) Rat brain membrane vesicles were incubated with increasing concentrations of [^{3}H]BPBTS. Specific binding data (□) were assessed from the difference between total (●) and nonspecific (■) binding. For this experiment a K_d of 5.2 nM and a B_{max} of 7.8 pmol/mg of protein were determined. (B) Rat brain membranes were incubated with 2.45 nM [^{3}H]BPBTS for the indicated periods of time. Nonspecific binding was time invariant and has been subtracted from the experimental points. Inset: Linear transformation of specific binding data according to the pseudo-first-order reaction yielded $k_{obs} = 0.012$ min^{-1}, corresponding to a k_1 of 2.3×10^4 M^{-1} s^{-1}. (C) Rat brain synaptosomal membranes were incubated with [^{3}H]BPBTS, and dissociation kinetics were initiated by addition of 1 (△), 2 (□), or 10 (○) μM unlabeled BPBTS. Data were fitted to a single monoexponential decay: (△) $k_{-1} = 0.022$ min^{-1}, (□) $k_{-1} = 0.043$ min^{-1}, (○) $k_{-1} = 0.14$ min^{-1}. (D) Rat brain membranes were incubated with ~1.3 nM [^{3}H]BPBTS in the presence of increasing concentrations of BPBTS (⊙), flunarizine (▲), R(+)SDZ-201 (▼), S(−)SDZ-201 (▽), quinidine (◆), veratridine (◇), deltamethrin (△), WIN 17317-3 (■), tetracaine (●), lidocaine (×), or phenytoin (□) for 20 h at room temperature. Specific binding data were fitted to a single-site inhibition model, yielding IC_{50} values of (⊙) 6.5 nM, (▲) 7.8 nM, (▼) 8 nM, (▽) 9.5 nM, (◆) 1.5 μM, (◇) 10 μM, (■) 1.4 nM, (●) 600 nM, and (×) 60 μM.

(Figure 3B), yielding $K_r = 2.8 \pm 0.4$ μM ($n = 7$). Inhibition was more pronounced when currents were activated from more depolarized holding potentials, resulting in an average shift in the steady-state availability curve of -13.7 ± 1.5 mV and an average K_i of 25 ± 9 nM ($n = 7$).

Binding of [^{3}H]BPBTS to Rat Brain Membranes. To gain more insight into the interactions of BPBTS with voltage-gated sodium channels, BPBTS was radioloabeled with tritium, and its properties of binding to a well-characterized preparation of sodium channels were determined. Under equilibrium conditions, specific binding of [^{3}H]BPBTS to rat brain synaptosomal membranes was saturable (Figure 4A) and was fitted to a single-site model with a K_d of 6.1 ± 0.8 nM and a Hill coefficient of 0.85 ± 0.17 ($n = 5$). The B_{max} obtained in this membrane preparation, 7.8 pmol/mg of protein, was similar to that of other sodium channel ligands, such as [^{3}H]WIN 17317-3 (*27*). Unlabeled BPBTS displaced [^{3}H]BPBTS binding to brain membranes with a K_i value of 6.3 ± 0.4 nM and a Hill slope of 0.96 ± 0.08 ($n = 12$) (Figure 4D).

The kinetics of [^{3}H]BPBTS binding to rat brain membranes were evaluated to determine whether ligand association occurs through a simple bimolecular reaction. Binding of 2.7 nM [^{3}H]BPBTS was a time-dependent process that reached equilibrium in approximately 4 h at room temperature (Figure 4B). Linear transformation of these data, according to a pseudo-first-order reaction, yielded a k_{obs} of 0.012 min^{-1}, corresponding to an association rate constant, k_1, of 2.3×10^4 M^{-1} s^{-1}. Dissociation of receptor-bound ligand, initiated by addition of excess unlabeled ligand, closely followed monoexponential kinetics, in agreement with a first-order reaction (Figure 4C). Interestingly, the rate of dissociation depended on the concentration of unlabeled ligand used to block association of the radioligand. Thus, when dissociation rates were examined in the presence of 1 μM unlabeled ligand (a concentration that should have been sufficient to saturate all high-affinity sites), k_{-1} values of 0.02 min^{-1} were obtained, but when 2 or 10 μM unlabeled ligand was used, dissociation rates were approximately 2- and 7-fold faster (k_{-1} of 0.04 and 0.14 min^{-1}, respectively). Such data have been interpreted as the result of multiple attachment points between the ligand and its receptor (*39*).

The pharmacology of [^{3}H]BPBTS binding to rat brain membranes was investigated using different classes of sodium channel modulators. All compounds tested were found to inhibit the interaction of [^{3}H]BPBTS with brain membranes (Figure 4D) and to display K_i values similar to those found in competition experiments with other well-

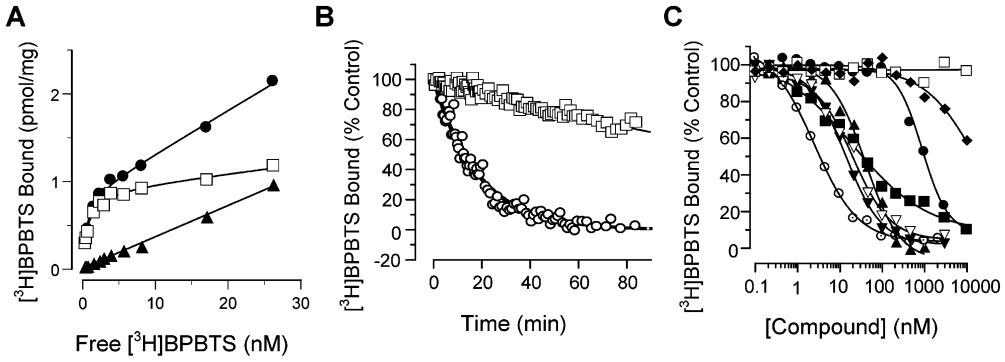

FIGURE 5: Binding of [^{3}H]BPBTS to hNa$_V$1.5 membranes. (A) Membranes prepared from HEK293 cells stably transfected with hNa$_V$1.5 were incubated with increasing concentrations of [^{3}H]BPBTS. Specific binding data (□) were assessed from the difference between total (●) and nonspecific (▲) binding. For this experiment a K_d of 0.9 nM and a B_{max} of 1.3 pmol/mg of protein were determined. (B) Na$_V$1.5 membranes were incubated with [^{3}H]BPBTS at room temperature, and dissociation kinetics were initiated by addition of 1 (□) or 10 (○) μM unlabeled BPBTS. Specific binding data were fitted to a single monoexponential decay: (□) $k_{-1} = 0.005$ min^{-1}, (○) $k_{-1} = 0.053$ min^{-1}. (C) Membranes were incubated with ~1.2 nM [^{3}H]BPBTS in the presence of increasing concentrations of BPBTS (⊙), flunarizine (▲), R(+)SDZ-201 (▼), S(−)SDZ-201 (▽), quinidine (◆), WIN 17317-3 (■), tetracaine (●), or phenytoin (□) for 20 h at room temperature. Specific binding data were fitted to a single-site inhibition model, yielding IC$_{50}$ values of (⊙) 2.5 nM, (▲) 36 nM, (▼) 14 nM, (▽) 21 nM, (■) 23 nM, and (●) 914 nM.

characterized sodium channel ligands, such as [^{3}H]WIN 17317-3 and [^{3}H]batrachotoxin (*24*). The compounds evaluated include sodium channel agonists (veratridine, $K_i = 8.4$ μM; deltamethrin), an antiarrhythmic agent (quinidine, $K_i = 1.3$ μM), cardiotonic agents (R(+)SDZ-201, $K_i = 6.8$ nM; S(−)SDZ-201, $K_i = 8$ nM), a calcium channel modifier (flunarizine, $K_i = 6.4$ nM), local anesthetics (tetracaine, $K_i = 430$ nM; lidocaine, $K_i = 44$ μM), an anticonvulsant (phenytoin, $K_i > 5$ μM), and the sodium channel blocker WIN 17317-3 ($K_i = 1.1$ nM). Most compounds produced complete inhibition of [^{3}H]BPBTS binding with the exception of deltamethrin, which inhibited binding by approximately 40%, and phenytoin, which inhibited about 30% of [^{3}H]-BPBTS binding at 10 μM. Other ion channel modulators, not known to block sodium channels, were also tested for their ability to displace [^{3}H]BPBTS binding from rat brain membranes. They include the selective K_V1.3 inhibitor correolide, the K_{Ca}1.1 (BK) channel inhibitor penitrem A, the L-type calcium channel blocker nitrendipine, the K_{ATP} blocker glibenclamide, and the anticonvulsant gabapentin. These agents caused only modest inhibition of [^{3}H]BPBTS binding when tested at 10 μM: 7%, 55%, 26%, 6%, and 0% inhibition for correolide, penitrem A, nitrendipine, glibenclamide, and gabapentin, respectively. Taken together, these data suggest that [^{3}H]BPBTS binds to a single class of high-affinity sites in rat brain membranes that display the pharmacological properties expected for voltage-gated sodium channels.

Binding of [^{3}H]BPBTS to Heterologously Expressed Sodium Channels. The interaction of [^{3}H]BPBTS with human cardiac, voltage-gated sodium channels was characterized in HEK-293 cells stably transfected with hNa$_V$1.5. Binding of [^{3}H]BPBTS to membranes derived from this cell line was consistent with a single class of sites with $K_d = 0.88 \pm 0.08$ nM ($n = 3$) and a B_{max} of 1.3 pmol/mg of protein (Figure 5A). Unlabeled BPBTS displaced [^{3}H]BPBTS binding to Na$_V$1.5 membranes with a K_i value of 1.45 ± 0.15 nM ($n = 2$), and a Hill slope of 1 (Figure 5C). Dissociation of ligand-bound receptor initiated by addition of 1 μM unlabeled ligand followed monoexponential kinetics with $k_{-1} = 0.0049$ min^{-1} (Figure 5B). This value is approximately 4-fold different from that determined for rat brain membranes (see above) and is consistent with the ~6-fold higher affinity of [^{3}H]-BPBTS for Na$_V$1.5 determined in equilibrium binding studies. Rates of ligand dissociation from Na$_V$1.5 displayed cooperative behavior similar to that observed with rat brain sodium channels. Thus, when dissociation was initiated by addition of 10 μM unlabeled ligand, a k_{-1} value of 0.053 min^{-1} was obtained. This value is about 10-fold higher than that determined in the presence of 1 μM unlabeled ligand. Binding of [^{3}H]BPBTS to Na$_V$1.5 membranes was inhibited, in a concentration-dependent manner, by flunarizine ($K_i = 14.5$ nM), tetracaine ($K_i = 368$ nM), WIN 17317-3 ($K_i = 7.8$ nM), R(+)SDZ-201 ($K_i = 7.5$ nM), or S(−)SDZ-201 ($K_i = 11.3$ nM), whereas phenytoin did not affect ligand binding, and quinidine displayed an IC$_{50} > 10$ μM (Figure 5C).

Formalin Test. The analgesic potential of BPBTS was tested in the formalin test, a rat model of tonic pain. Intraplantar injection of formalin in vehicle-treated animals resulted in two phases of spontaneous pain behavior as evidenced by flinching and paw licking (Figure 6A). Intradermal administration of 150 μg of BPBTS had no effect on pain behavior during the first phase of the test (1−10 min), but inhibited flinching behavior from 10 to 50 min during the late phase. Compared to vehicle, injection of 150 μg of BPBTS inhibited the number of flinches during the late phase, measured as the area under the curve represented in Figure 6A, by 46% ($P < 0.01$). Inhibition of late-phase formalin-induced flinching by BPBTS was dose-dependent, with a 1.5 μg dose producing 16% inhibition, which was not statistically significant (Figure 6B). Intravenous administration of 10 mg/kg BPBTS 5 min prior to formalin injection produced significant inhibition of both phases of nociceptive behavior ($P < 0.05$). Compared with administration of vehicle alone, flinching behavior during the early and late phases was inhibited by 48% and 33%, respectively (Figure 6C). Since formalin-induced nociceptive behavior during the late phase is dependent on afferent input during the early phase, BPBTS (10 mg/kg iv) was administered 15 min after the formalin challenge to dissociate late-phase from early-phase inhibition (Figure 6C). In this dosing regimen, flinching behavior during the early phase of the test was comparable in vehicle- and BPBTS-treated rats, yet BPBTS still attenuated flinching during the first half of the late phase

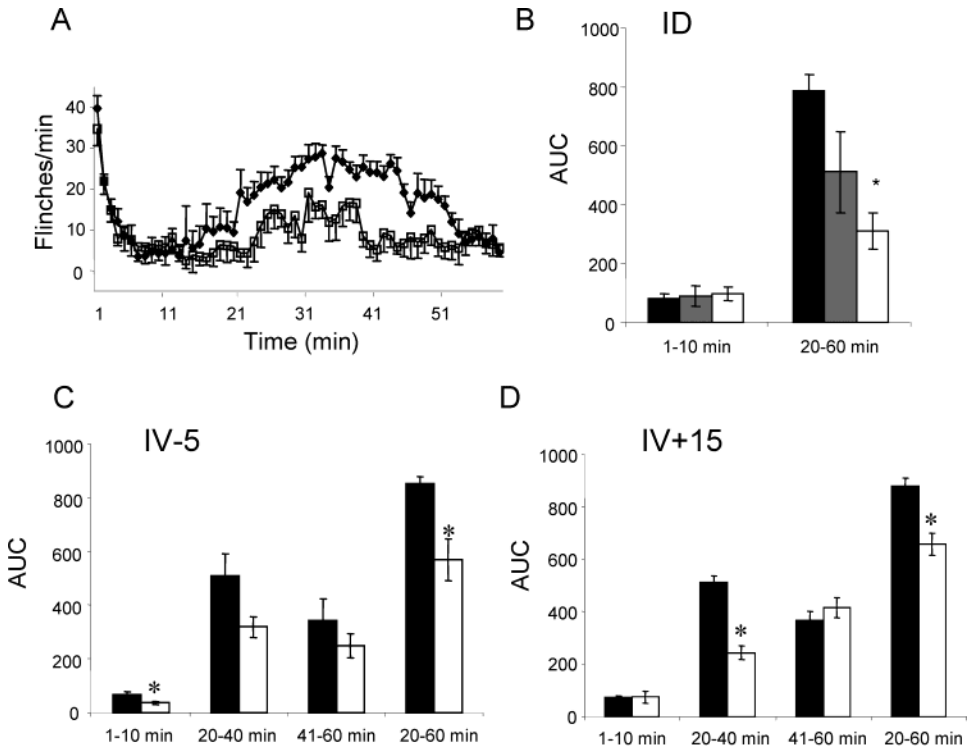

FIGURE 6: BPBTS reduced formalin-induced flinching behavior in rats. (A) Number of flinches per minute as a function of time after subcutaneous formalin injection. Data shown are averages and standard errors for 16 vehicle-treated animals (◆) and 15 animals intradermally injected with 150 μg of BPBTS (□). (B) Intradermal injection of BPBTS. Bar graph showing the area under the flinches-vs-time curve (AUC) for the first (1−10 min) and second (20−60 min) phases of the test. Vehicle-treated animals ($n = 16$) are shown in black, animals injected with 1.5 μg in gray ($n = 5$), and animals injected with 150 μg ($n = 15$) in white. (C) Intravenous administration of BPBTS 5 min prior to formalin challenge. Shown are the AUCs for the first (1−10 min) and second (20−60 min) phases of the test, with vehicle-treated animals ($n = 6$) in black and animals administered 10 mg/kg BPBTS ($n = 4$) in white. (D) Intravenous administration of BPBTS 15 min after formalin injection. Shown are the AUCs for the first and second phases of the test, with vehicle-treated animals ($n = 20$) in black and animals administered 10 mg/kg BPBTS ($n = 9$) in white.

by 52% ($P < 0.05$). Approximately 30 min after dosing with BPBTS (40−60 min), nociceptive behavior returned to that observed in vehicle-treated animals. The short duration of the analgesic effect can be attributed to the poor pharmacokinetic properties of the compound (mean residence time 0.23 h).

DISCUSSION

Reported in this study is the identification of BPBTS as a potent sodium channel inhibitor. BPBTS inhibited all Na_V1 channels tested ($Na_V1.2$, $Na_V1.5$, and $Na_V1.7$), as well as the TTX-resistant sodium current in dissociated dorsal root ganglia, and, on the basis of binding assays, appeared selective for Na_V1 channels over the calcium and potassium channels tested. Block of Na_V1 channels by BPBTS was both state- and frequency-dependent, features associated with the therapeutic window of sodium channel blockers. BPBTS displayed efficacy in a pain model in vivo, suggesting its usefulness as a lead compound for development of future analgesics.

The discovery of BPBTS emphasizes the utility of the VIPR assay, as a high-throughput functional assay for identifying sodium channel blockers. Since it measures membrane depolarization, the VIPR assay is expected to be highly nonlinear. Interestingly, the IC_{50} values obtained in the VIPR assay for BPBTS, as well as for a number of standard sodium channel blockers, were very similar to the affinity of these compounds for the inactivated state of the channel (K_i) determined in whole cell electrophysiology.

State-dependent sodium channel blockers have demonstrated therapeutic utility as anticonvulsants, antiarrhythmics, and local anesthetics, and more recently as treatments for a number of neuropathic pain conditions. In addition, sodium channel blockers have been investigated as treatments for stroke, bipolar disease, and multiple sclerosis. Despite the rich therapeutic potential, few novel chemical entities have been revealed since the empirical discoveries of currently used agents such as lamotrigine and lidocaine. Sodium channel blockers currently used in the clinic are associated with a number of side effects, which become dose-limiting and prevent patients from achieving adequate treatment. Except for rare occurrences of Stevens−Johnson syndrome with lamotrigine, dose-limiting side effects typically result from sodium channel block in the central nervous system and include ataxia and sedation. Currently used agents are relatively weak sodium channel blockers and highly brain penetrant, emphasizing the need for more potent and selective and potentially less brain penetrant therapies. Although none of the clinically used sodium channel blockers are subtype-selective, few cardiac side effects have been reported in patients without prior heart conditions.

The biophysical properties of BPBTS action on sodium channels suggest a mechanism of block similar to that of lidocaine. BPBTS appears to bind predominantly to channels in open and inactivated states. At the resting membrane potential of peripheral nerves, the majority of sodium channels are expected to reside in the resting state and thus to open normally during brief depolarizations, minimizing

the impact on normal nerve conduction. However, when cells become depolarized, channels accumulate in the inactivated state where high-affinity binding of BPBTS will make them unavailable for subsequent opening. BPBTS is therefore expected to reduce excitability specifically under conditions such as ischemia and tissue injury or during rapid firing.

The guanidinium toxins TTX and STX have been valuable tools in characterizing sodium channels and investigating their structure and physiological roles. However, TTX and STX bind with very low affinity to the more recently cloned sodium channel subtypes $Na_V1.8$ and $Na_V1.9$. On the basis of its voltage dependence and kinetics, the native TTX-resistant current in DRGs is thought to be carried by $Na_V1.8$ channels (*1*, *19*, *20*), making BPBTS a potential high-affinity ligand of these channels. The availability of a radioligand for $Na_V1.8$ could be an important tool in the generation of stable cell lines and potentially in the search for subtype-selective blockers. Other radioligands that bind to voltage-gated sodium channels have been identified, but [^{3}H]BTX-B requires coapplication of scorpion toxin to enhance specific binding, which may complicate the resulting pharmacology (*24*), and [^{3}H]WIN 17317-3 and [^{3}H]lifarizine are not selective for sodium channels over certain potassium or calcium channels, respectively (*27*, *40*). In addition, some properties of [^{3}H]BPBTS binding, namely, the dependence of ligand dissociation rate on competing ligand concentration, have not been reported previously for other sodium channel probes, suggesting a unique mechanism of interaction of BPBTS with the channel.

The formalin test (*41*) is commonly used to assess the antinociceptive efficacy of drugs in rats and mice. Injection of a dilute solution of formalin into the paw activates C-fibers in a biphasic manner and induces two distinct phases of pain behavior (*42*). Intravenous administration of lidocaine reduces formalin-induced C-fiber activity without affecting conduction of electrical or mechanical stimuli. This inhibition of peripheral nerve activity is achieved at plasma concentrations similar to those required to inhibit pain behavior in rats and relieve neuropathic pain in patients (*43*). Several other sodium channel blockers, including the anticonvulsants lamotrigine and carbamazepine and the antiarrhythmic mexiletine, have been shown to inhibit nociceptive behavior in response to formalin injection (*44*), and the same sodium channel blockers are used to treat neuropathic pain.

Clinically used sodium channel blockers preferentially bind to the open and inactivated states of sodium channels. BPBTS shares this mechanism, but is approximately 2 orders of magnitude more potent than currently available drugs, suggesting that BPBTS might be a promising lead for developing novel analgesics. The primary deficiencies of BPBTS, which will have to be addressed in future analogues, are the poor pharmacokinetic profile and the potent block of resting and inactivated $Na_V1.5$ channels. Analogues with better pharmacokinetic properties are expected to provide insight into the therapeutic index of this novel class of sodium channel blockers.

ACKNOWLEDGMENT

We thank Franz Hofmann for the $hNa_V1.7$ cDNA and Hali Hartmann for the cDNA and HEK cells expressing $hNa_V1.5$. Further, we thank Owen McManus and Robert Slaughter for advice and helpful discussions throughout the course of these experiments.

REFERENCES

1. Goldin, A. L., Barchi, R. L., Calwell, J. H., Hofmann, F., Howe, J. R., Hunter, J. C., Kallen, R. G., Mandel, G., Meisler, M. H., Netter, Y. B., Noda, M., Tamkun, M. M., Waxman, S. G., Wood, J. N., and Catterall, W. A. (2000) Nomenclature of voltage-gated sodium channels, *Neuron 28*, 165−368.
2. Catterall, W. A., Goldin, A. L., Waxman, S. G., and International-Union-of-Pharmacology. (2003) International Union of Pharmacology. XXXIX. Compendium of voltage-gated ion channels: sodium channels, *Pharmacol. Rev. 55*, 575−8.
3. Catterall, W. A. (1992) Cellular and molecular biology of voltage-gated sodium channels, *Physiol. Rev. 72*, S15−48.
4. Isom, L. L. (2001) Sodium channel beta subunits: anything but auxiliary, *Neuroscientist 7*, 42−54.
5. Isom, L. L., Ragsdale, D. S., De-Jongh, K. S., Westenbroek, R. E., Reber, B. F., Scheuer, T., and Catterall, W. A. (1995) Structure and function of the beta 2 subunit of brain sodium channels, a transmembrane glycoprotein with a CAM motif, *Cell 83*, 433−42.
6. Shah, B. S., Stevens, E. B., Gonzalez, M. I., Bramwell, S., Pinnock, R. D., Lee, K., and Dixon, A. K. (2000) beta3, a novel auxiliary subunit for the voltage-gated sodium channel, is expressed preferentially in sensory neurons and is upregulated in the chronic constriction injury model of neuropathic pain, *Eur. J. Neurosci. 12*, 3985−90.
7. Isom, L. L., De Jongh, K. S., Patton, D. E., Reber, B. F., Offord, J., Charbonneau, H., Walsh, K., Goldin, A. L., and Catterall, W. A. (1992) Primary structure and functional expression of the beta 1 subunit of the rat brain sodium channel, *Science 256*, 839−42.
8. Vijayaragavan, K., O'Leary, M. E., and Chahine, M. (2001) Gating properties of Na(v)1.7 and Na(v)1.8 peripheral nerve sodium channels, *J. Neurosci. 21*, 7909−18.
9. Clare, J. J., Tate, S. N., Nobbs, M., and Romanos, M. A. (2000) Voltage-gated sodium channels as therapeutic targets, *Drug Discovery Today 5*, 506−520.
10. Zimanyi, I., Weiss, S. R., Lajtha, A., Post, R. M., and Reith, M. E. (1989) Evidence for a common site of action of lidocaine and carbamazepine in voltage-dependent sodium channels, *Eur. J. Pharmacol. 167*, 419−22.
11. Ragsdale, D. S., McPhee, J. C., Scheuer, T., and Catterall, W. A. (1996) Common molecular determinants of local anesthetic, antiarrhythmic, and anticonvulsant block of voltage-gated Na+ channels, *Proc. Natl. Acad. Sci. U.S.A. 93*, 9270−5.
12. Kohling, R. (2002) Voltage-gated sodium channels in epilepsy, *Epilepsia 43*, 1278−95.
13. Scholz, A. (2002) Mechanisms of (local) anaesthetics on voltage-gated sodium and other ion channels, *Br. J. Anaesth. 89*, 52−61.
14. di-Vadi, P. P., and Hamann, W. (1998) The use of lamotrigine in neuropathic pain, *Anaesthesia 53*, 808−9.
15. Rizzo, M. A. (1997) Successful treatment of painful traumatic mononeuropathy with carbamazepine: insights into a possible molecular pain mechanism, *J. Neurol. Sci. 152*, 103−6.
16. Ross, E. L. (2000) The evolving role of antiepileptic drugs in treating neuropathic pain, *Neurology 55*, S41−6; discussion S54−8.
17. Argoff, C. E. (2000) New analgesics for neuropathic pain: the lidocaine patch, *Clin. J. Pain 16*, 62−66.
18. Noda, M., Shimizu, S., Tanabe, T., Takai, T., Kayano, T., Ikeda, T., Takahashi, H., Nakayama, H., Kanaoka, Y., Minamino, N., and et al. (1984) Primary structure of Electrophorus electricus sodium channel deduced from cDNA sequence, *Nature 312*, 121−7.
19. Sangameswaran, L., Delgado, S. G., Fish, L. M., Koch, B. D., Jakeman, L. B., Stewart, G. R., Sze, P., Hunter, J. C., Eglen, R. M., and Herman, R. C. (1996) Structure and function of a novel voltage-gated, tetrodotoxin-resistant sodium channel specific to sensory neurons, *J. Biol. Chem. 271*, 5953−6.
20. Akopian, A. N., Sivilotti, L., and Wood, J. N. (1996) A tetrodotoxin-resistant voltage-gated sodium channel expressed by sensory neurons, *Nature 379*, 257−62.
21. Tate, S., Benn, S., Hick, C., Trezise, D., John, V., Mannion, R. J., Costigan, M., Plumpton, C., Grose, D., Gladwell, Z., Kendall, G., Dale, K., Bountra, C., and Woolf, C. J. (1998) Two sodium

channels contribute to the TTX-R sodium current in primary sensory neurons, *Nat. Neurosci. 1*, 653−5.
22. Dib-Hajj, S. D., Tyrrell, L., Black, J. A., and Waxman, S. G. (1998) NaN, a novel voltage-gated Na channel, is expressed preferentially in peripheral sensory neurons and down-regulated after axotomy, *Proc. Natl. Acad. Sci. U.S.A. 95*, 8963−8.
23. Satin, J., Kyle, J. W., Chen, M., Bell, P., Cribbs, L. L., Fozzard, H. A., and Rogart, R. B. (1992) A mutant of TTX-resistant cardiac sodium channels with TTX-sensitive properties, *Science 256*, 1202−5.
24. Catterall, W. A., Morrow, C. S., Daly, J. W., and Brown, G. B. (1981) Binding of batrachotoxinin A 20-alpha-benzoate to a receptor site associated with sodium channels in synaptic nerve ending particles, *J. Biol. Chem. 256*, 8922−7.
25. Gonzalez, J. E., Oades, K., Leychkis, Y., Harootunian, A., and Negulescu, P. A. (1999) Cell-based assays and instrumentation for screening ion-channel targets, *Drug Discovery Today 4*, 431−439.
26. Schroeder, K., Neagle, B., Trezise, D. J., and Worley, J. (2003) Ionworks HT: a new high-throughput electrophysiology measurement platform, *J. Biomol. Screening 8*, 50−64.
27. Wanner, S. G., Glossmann, H., Knaus, H. G., Baker, R., Parsons, W., Rupprecht, K. M., Brochu, R., Cohen, C. J., Schmalhofer, W., Smith, M., Warren, V., Garcia, M. L., and Kaczorowski, G. J. (1999) WIN 17317−3, a new high-affinity probe for voltage-gated sodium channels, *Biochemistry 38*, 11137−46.
28. Gonzalez, J. E., and Maher, M. P. (2002) Cellular fluorescent indicators and voltage/ion probe reader (VIPR) tools for ion channel and receptor drug discovery, *Recept. Channels 8*, 283−95.
29. Middleton, R. E., Warren, V. A., Kraus, R. L., Hwang, J. C., Liu, C. J., Dai, G., Brochu, R. M., Kohler, M. G., Gao, Y. D., Garsky, V. M., Bogusky, M. J., Mehl, J. T., Cohen, C. J., and Smith, M. M. (2002) Two tarantula peptides inhibit activation of multiple sodium channels, *Biochemistry 41*, 14734−47.
30. Hamill, O. P., Marty, A., Neher, E., Sakmann, B., and Sigworth, F. J. (1981) Improved patch-clamp techniques for high-resolution current recording from cells and cell-free membrane patches, *Pfluegers Arch. 391*, 85−100.
31. Bean, B. P., Cohen, C. J., and Tsien, R. W. (1983) Lidocaine block of cardiac sodium channels, *J. Gen. Physiol. 81*, 613−42.
32. Ashton, W. T., Chang, L. L., Flanagan, K. L., Hutchins, S. M., Naylor, E. M., Chakravarty, P. K., Patchett, A. A., Greenlee, W. J., Chen, T. B., Faust, K. A., and et al. (1994) Triazolinone biphenylsulfonamide derivatives as orally active angiotensin II antagonists with potent AT1 receptor affinity and enhanced AT2 affinity, *J. Med. Chem. 37*, 2808−24.
33. Knaus, H. G., Koch, R. O., Eberhart, A., Kaczorowski, G. J., Garcia, M. L., and Slaughter, R. S. (1995) [125I]margatoxin, an extraordinarily high affinity ligand for voltage-gated potassium channels in mammalian brain, *Biochemistry 34*, 13627−34.
34. Klugbauer, N., Lacinova, L., Flockerzi, V., and Hofmann, F. (1995) Structure and functional expression of a new member of the tetrodotoxin-sensitive voltage-activated sodium channel family from human neuroendocrine cells, *EMBO J. 14*, 1084−90.
35. White, M. M., Chen, L. Q., Kleinfield, R., Kallen, R. G., and Barchi, R. L. (1991) SkM2, a Na+ channel cDNA clone from denervated skeletal muscle, encodes a tetrodotoxin-insensitive Na+ channel, *Mol. Pharmacol. 39*, 604−8.
36. Gellens, M. E., George, A. L., Jr., Chen, L. Q., Chahine, M., Horn, R., Barchi, R. L., and Kallen, R. G. (1992) Primary structure and functional expression of the human cardiac tetrodotoxin-insensitive voltage-dependent sodium channel, *Proc. Natl. Acad. Sci. U.S.A. 89*, 554−8.
37. Gold, M. S. (1999) Tetrodotoxin-resistant Na+ currents and inflammatory hyperalgesia, *Proc. Natl. Acad. Sci. U.S.A. 96*, 7645−9.
38. Lai, J., Gold, M. S., Kim, C. S., Bian, D., Ossipov, M. H., Hunter, J. C., and Porreca, F. (2002) Inhibition of neuropathic pain by decreased expression of the tetrodotoxin-resistant sodium channel, NaV1.8, *Pain 95*, 143−52.
39. Prinz, H., and Striessnig, J. (1993) Ligand-induced accelerated dissociation of (+)-cis-diltiazem from L-type Ca2+ channels is simply explained by competition for individual attachment points, *J. Biol. Chem. 268*, 18580−5.
40. MacKinnon, A. C., Wyatt, K. M., McGivern, J. G., Sheridan, R. D., and Brown, C. M. (1995) [3H]-lifarizine, a high affinity probe for inactivated sodium channels, *Br. J. Pharmacol. 115*, 1103−9.
41. Dubuisson, D., and Dennis, S. G. (1977) The formalin test: a quantitative study of the analgesic effects of morphine, meperidine, and brain stem stimulation in rats and cats, *Pain 4*, 161−174.
42. McCall, W. D., Tanner, K. D., and Levine, J. D. (1996) Formalin induces biphasic activity in C-fibers in the rat, *Neurosci. Lett. 208*, 45−8.
43. Puig, S., and Sorkin, L. S. (1996) Formalin-evoked activity in identified primary afferent fibers: systemic lidocaine suppresses phase-2 activity, *Pain 64*, 345−55.
44. Blackburn-Munro, G., Ibsen, N., and Erichsen, H. K. (2002) A comparison of the anti-nociceptive effects of voltage-activated Na+ channel blockers in the formalin test, *Eur. J. Pharmacol. 445*, 231−238.

BI0493259